Reversal in Failure Scaling Transition of Fibrous Composites

By Alberto Carpinteri,[1] Fellow, ASCE, and Roberta Massabó[2]

Abstract: A nonlinear fracture mechanics model is proposed for analysis of the flexural behavior of brittle-matrix composites with uniformly distributed secondary phases. In accordance with the Barenblatt-Dugdale model the bridging or cohesive zone of the material is replaced by a fictitious crack along which a closing traction distribution is applied. The dimensionless formulation brings out the parameters synthetically controlling the structural behavior and the size-scale effects. Different scaling transitions are predicted in the flexural behavior of the composite depending on different modeling of the toughening mechanisms. When a homogenized toughening mechanism for the whole composite is considered along with closing tractions as a linearly decreasing function of the crack opening displacement, a ductile to brittle transition is found as the beam depth increases. On the other hand, when the matrix toughness and the toughening mechanism of the reinforcements are separately modeled, and the closing tractions have a constant value until a critical crack opening displacement, a double brittle-ductile-brittle transition is found. Experimental tests on fiber-reinforced mortar beams in bending are successfully simulated.

INTRODUCTION

In laboratory tests, strain-softening materials, such as cementitious composites, usually show a variation in the kind of flexural response, which changes from strain-hardening to strain-softening when the size of the samples is increased (Bosco et al. 1990). On the other hand, brittle-matrix fiber-reinforced composites, such as typical fiber-reinforced cementitious materials, show an opposite transition from strain-softening to strain-hardening when a characteristic dimension of the sample is increased (Jamet et al., in press, 1996).

The previously mentioned materials are characterized by an internal crack controlling mechanism exerted by the secondary phases (aggregates, fibers, particles). The secondary phases bridge the macrocracks along their wake and the microcracks in the process zone ahead of the macrocracks, thus preventing their coalescence, opening, and propagation.

Two analytical approaches, based on fracture mechanics concepts, are used to analyze the composite failure process: the bridged-crack model, which assumes a nonvanishing crack-tip stress intensity factor, and the cohesive-crack model, which assumes a vanishing stress intensity factor. Numerous theoretical models, derived from the models of Barenblatt (1959, 1962) and Dugdale (1960), have been proposed (Cox and Marshall 1994). Many of these are concerned with the flexural behavior of composites used in civil engineering applications, such as concrete and mortar (Hillerborg et al. 1976; Jenq and Shah 1985; Shah 1988; Carpinteri 1989; Cotterel et al. 1992), fiber-reinforced cementitious materials (Wecharatana and Shah 1983; Visalvanich and Naaman 1983; Ballarini et al. 1984; Mai 1985; Jenq and Shah 1986; Foote et al. 1986; Li and Liang 1986; Hillerborg 1989; Carpinteri and Massabó 1995), and reinforced concrete (Romualdi and Batson 1963; Carpinteri 1984; Desayi and Ganesan 1986; Bosco and Carpinteri 1992, 1995).

In this paper a nondimensional fracture mechanics model is proposed for analysis of the flexural behavior of brittle-matrix composites with uniformly distributed secondary phases. The potential crises due to brittle crack propagation in the matrix and due to yielding, debonding, or pulling-out of the reinforcements are considered. The mechanical behavior of the member in flexure is deduced from these elementary events. The theoretical formulation is derived from the discontinuous model proposed by Bosco and Carpinteri (1995) for the analysis of composites with a discrete number of localized reinforcements. The nonlinear problem has been solved using the stress intensity factor superposition principle and the localized compliances due to the crack in the evaluation of the displacements for the verification of kinematic compatibility.

The dimensionless parameters that control the nonlinear behavior of the composite are defined, and the size-scale effect in a generic brittle-matrix composite is predicted. The theoretical model provides an explanation of, and renders reproducible, the scaling transitions in the shape of the flexural constitutive relationship shown by cementitious materials and fibrous composites in laboratory tests. Finally, the theoretical model is applied to simulate some experimental tests carried out on fiber-reinforced mortar beams in bending.

THEORETICAL MODEL

The proposed theoretical model analyzes the evolutive process of crack propagation in a brittle-matrix composite cross section in bending to define the constitutive flexural relationship that characterizes the mechanical response of the member. Fig. 1, representing the cracked cross section of a beam of depth h and thickness b, is considered. In accordance with the models of Barenblatt (1959, 1962) and Dugdale (1960), the crack of depth a consists of a traction-free part of depth a_r and a fictitious part of depth a_f, acted upon by the closing tractions σ_0. The fictitious crack can represent either a microcracked process zone ahead of a macrocrack or a macrocrack wake bridged by reinforcing elements. The normalized crack depths $\xi = a/h$; $\xi_r = a_r/h$; and $\xi_f = a_f/h$ are defined together with the normalized value $\zeta = x/h$ of the generic coordinate x related to the bottom of the cross section.

The uniformly distributed reinforcements are taken into account in the postcracking loading phase through the closing

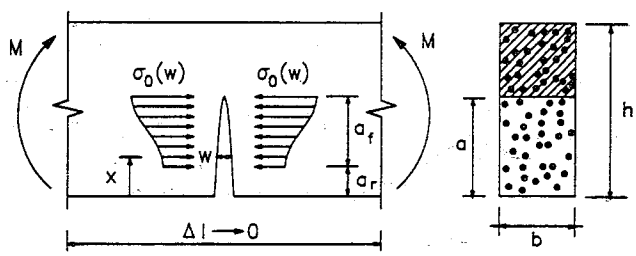

FIG. 1. Cracked Cross Section in Bending

[1]Prof., Dipartimento di Ingegneria Strutturale, Politecnico di Torino, Corso Duca degli Abruzzi, 24, 10129, Torino, Italy.

[2]Asst. Prof., Istituto di Scienza delle Costruzioni, Universitá di Genova, Via Montallegro, 1, 16145, Genova, Italy.

Note. Associate Editor: Robert Y. Liang. Discussion open until July 1, 1997. To extend the closing date one month, a written request must be filed with the ASCE Manager of Journals. The manuscript for this paper was submitted for review and possible publication on July 21, 1995. This paper is part of the ***Journal of Engineering Mechanics***, Vol. 123, No. 2, February, 1997. ©ASCE, ISSN 0733-9399/97/0002-0107–0114/ $4.00 + $.50 per page. Paper No. 11230.

tractions σ_0, which are linked to the crack profile $w(x)$, according to an assigned relationship $\sigma_0(w)$ (Fig. 1). If the reinforcements are present in a low volume ratio, the precracking response of the composite coincides with that of the matrix, which is assumed to be linear-elastic. The failure mechanism for compressive crushing is not considered.

The problem at hand is a nonlinear statically indeterminate one, the indeterminate closing tractions depend on the unknown crack opening displacements. The model has been formulated with two options. The first, called bridging option, is based on assumptions that fit the analytical formulation in the general framework of the bridged-crack model, for which a singular stress field is assumed at the crack tip. The second, or cohesive option, follows the assumptions of the general cohesive-crack model, which supposes a finite stress field in the crack tip vicinity. A unitary dimensionless formulation can be developed, provided the parameters appearing in the analytical relationships take on appropriate meanings in accordance to the option adopted.

Crack Propagation Condition

The bridging option represents the brittle-matrix composite as a multiphase material, and the parameters of the model relate to the different phases. The closing tractions σ_0 represent the bridging mechanism of the secondary phases, and the bridging relation $\sigma_0(w)$ is given by $\sigma_0(w) = \rho\sigma(w)$, ρ being the secondary-phase volume ratio and $\sigma(w)$ a function describing the bridging mechanism of the reinforcements. An approximate definition of the bridging relation can be obtained by simply extrapolating to all of the reinforcements the bridging relation $\sigma(w)$ deduced from experimental pull-out tests on a single reinforcement, or from analytical simulations of that test. It depends on the dimension and shape of the reinforcement, and on the properties at the interface.

Also the toughening mechanisms of the different phases are separately taken into account: the brittle-matrix fracture toughness, through a critical stress intensity factor K_{IC}, and the toughening mechanism of the secondary phases, through the shielding effect that the closing tractions develop on the crack tip stress intensification. At the tip of the crack a global stress intensity factor K_I can be evaluated through the superposition principle

$$K_I = K_{IM} - K_{I\sigma} \tag{1}$$

where K_{IM} and $K_{I\sigma}$ = stress intensity factors due to the applied bending moment M and to a distribution of opening tractions σ_0, respectively. The crack propagation condition sets the global crack tip stress intensity factor K_I equal to the critical value K_{IC}

$$K_{IM} - K_{I\sigma} = K_{IC} \tag{2}$$

The cohesive option represents the brittle-matrix composite as a monophase material, and the parameters of the model relate to the homogenized properties. The closing tractions $\sigma_0(w)$ describe the combined restraining action of the matrix and the secondary phases on the crack propagation. The cohesive relation $\sigma_0(w)$ is equal to the cohesive law $\sigma(w)$ deduced from direct tensile tests on the composite material. It depends on the mechanical properties of the matrix and the secondary phase, and on the dimension and shape of the latter. In this case only the global toughening mechanism of the composite is taken into account through the shielding effect of the closing tractions. The global crack tip stress intensity factor is given by (1), and it vanishes when the crack advances, as the matrix toughness has been included in $K_{I\sigma}$

$$K_{IM} - K_{I\sigma} = 0 \tag{3}$$

In accordance with the two-dimensional single-edge notched-strip solutions (Tada et al. 1985), the stress intensity factors in (2) and (3) are given in the following forms:

$$K_{IM} = \frac{M}{h^{1.5}b} Y_M(\xi) \tag{4}$$

$$K_{I\sigma} = \int_{\xi_r}^{\xi} \frac{K_{Ii}}{P_i} \sigma_0 [w(\zeta_i)] bh \, d\zeta_i = \frac{1}{h^{0.5}b} \int_{\xi_r}^{\xi} \sigma_0[w(\zeta_i)] Y_P(\xi, \zeta_i) bh \, d\zeta_i \tag{5}$$

where K_{Ii} = stress intensity factor due to two opening forces P_i, directly applied on the crack faces at the normalized coordinate ζ_i; and $Y_M(\xi)$ and $Y_P(\xi, \zeta_i)$ = polynominal functions related to the shape of the specimen.

The simplest bridging or cohesive relationships are the following power laws

$$\frac{\sigma}{\sigma_u} = 1 - \left(\frac{w}{w_c}\right)^n \tag{6a}$$

$$\frac{\sigma}{\sigma_u} = \left(\frac{w}{w_c}\right)^n \tag{6b}$$

These are characterized by the maximum traction σ_u, by the critical crack opening displacement w_c, beyond which the closing tractions vanish, and by the exponent n. For different values of the exponent n, the two laws can be used to simulate various bridging mechanisms.

Crack Propagation Moment

By means of (2)–(6), the crack-propagation moment for the two options can be evaluated as a function of the applied loads and the global crack depth. In dimensionless form it is given by

$$\frac{M_F}{K_{IC}h^{1.5}b} = \frac{1}{Y_M(\xi)} \left\{ B \int_{\xi_r}^{\xi} \frac{\sigma[w(\zeta)]}{\sigma_u} Y_P(\xi, \zeta) \, d\zeta + K \right\} \tag{7}$$

Bridging option:

$$K = 1; \quad B = N_P = \frac{\rho\sigma_u h^{0.5}}{K_{IC}} \tag{8}$$

Cohesive option:

$$K = 0; \quad B = \frac{1}{s} = \frac{\sigma_u h^{0.5}}{K_{IC}} \tag{9}$$

The parameters K and B, of (8) and (9), characterize the crack tip stress field and the brittleness of the cross section, respectively.

Under the bridging option, K_{IC} represents the matrix fracture toughness; $K = 1$ highlights the existence of a singular stress field at the crack tip; σ_u represents the ultimate strength of the reinforcements, or the maximum value of the bridging relation $\sigma(w)$; and $B = N_P$ is the brittleness number, formerly proposed by Carpinteri (1984) for the description of the failure mechanisms in reinforced concrete.

Under the cohesive option, K_{IC} represents the homogenized toughness of the composite; $K = 0$ highlights a finite stress field at the crack tip; σ_u is the homogenized ultimate strength of the composite, or the maximum value of the cohesive relation $\sigma(w)$; and $B = 1/s$ is the reciprocal of the brittleness number originally defined by Carpinteri (1981) for the description of the failure mechanisms in brittle homogeneous materials.

Flexural Constitutive Relationship

The localized rotation ϕ can be evaluated using the superposition principle and the localized compliances due to the crack

$$\phi = \phi_M - \phi_\sigma = \lambda_{MM}(\xi)M - \int_{\xi_r}^{\xi} \lambda_{Mi}(\xi, \zeta_i)\sigma_0[w(\zeta_i)]hb\, d\zeta_i \quad (10)$$

where ϕ_M and ϕ_σ = localized rotations due to the applied bending moment M and to the opening tractions $\sigma_0(w)$, respectively; and the localized compliances λ_{MM} and λ_{Mi} = rotations due to the crack produced, respectively, by a unit bending moment and by two unit opening forces, directly applied on the crack faces at the coordinate ζ_i.

The localized compliances can be deduced through an energy balance between the total potential energy W, released during the virtual formation of a unit increment of the crack surface area, and the crack driving force $\mathcal{G}$

$$\mathcal{G} = -\frac{1}{b}\frac{dW}{da} \quad (11)$$

If $\mathcal{G}$ is defined as a function of the local stress intensity factor K_I (Irwin's relation), and the total potential energy as a function of the applied loads and the corresponding displacements (Clapeyron's theorem), (11) leads to the following expressions (Bosco and Carpinteri 1992):

$$\lambda_{MM} = \frac{2bh}{E}\int_0^{\xi} \frac{K_{IM}^2}{M^2}\, d\xi = \frac{2}{Eh^2b}\int_0^{\xi} Y_M^2(\xi)\, d\xi \quad (12)$$

$$\lambda_{Mi} = \frac{2hb}{E}\int_{\zeta_i}^{\xi} \frac{K_{Ii}K_{IM}}{P_iM}\, d\xi = \frac{2}{Ehb}\int_{\zeta_i}^{\xi} Y_P(\xi, \zeta_i)Y_M(\xi)\, d\xi \quad (13)$$

The localized rotation at the onset of propagation is obtained by substituting (7), (12), and (13) into (10)

$$\phi = \frac{2K_{IC}}{Eh^{0.5}}\left\{\frac{M_F}{K_{IC}h^{1.5}b}\int_0^{\xi} Y_M^2(\xi)\, d\xi - B\int_{\xi_r}^{\xi}\left[\int_{\zeta}^{\xi} Y_M(y)Y_P(y, \zeta)\, dy\right]\frac{\sigma[w(\zeta)]}{\sigma_u}\, d\zeta\right\} \quad (14)$$

Once the bridging or cohesive relation $\sigma_0(w)$ has been assigned, and the mechanical and geometrical properties of the cross section have been fixed by means of the dimensionless numbers N_P or s, the constitutive flexural relationship, which is given by (7) and (14) by varying the crack depth, depends on the unknown closing tractions σ_0, which are functions of the crack profile $w(x)$, and on the normalized depth of the traction-free crack ξ_r, at the lower limit of the integrals in (7) and (14). The crack opening displacement $w(\zeta_k)$, at the generic normalized coordinate ζ_k, is

$$w(\zeta_k) = w_M(\zeta_k) - w_\sigma(\zeta_k) = \lambda_{kM}(\xi, \zeta_k)M - \int_{\xi_r}^{\xi} \lambda_{ki}(\xi, \zeta_k, \zeta_i)\sigma_0[w(\zeta_i)]hb\, d\zeta_i \quad (15)$$

where $w_M(\zeta_k)$ and $w_\sigma(\zeta_k)$ = crack opening displacements produced by the bending moment M and by the opening tractions σ_0, respectively. The compliances λ_{kM} and λ_{ki} = crack opening displacements at the coordinate ζ_k produced by a unit bending moment $M = 1$, (13), and by two unit concentrated forces applied at the generic coordinate ζ_i, respectively. The localized compliance λ_{ki} can be given the form

$$\lambda_{ki} = \frac{2hb}{E}\int_{\max[\zeta_k,\zeta_i]}^{\xi} \frac{K_{Ik}K_{Ii}}{P_kP_i}\, d\xi = \frac{2}{Eb}\int_{\max[\zeta_k,\zeta_i]}^{\xi} Y_P(\xi, \zeta_k)Y_P(\xi, \zeta_i)\, d\xi \quad (16)$$

The normalized value of the crack opening displacement for the crack at the onset of propagation $\tilde{w}_k = w_k/h$ is given by (7) and (15)

$$\tilde{w}(\zeta_k) = \frac{2K_{IC}}{Eh^{0.5}}\left\{\frac{M_F}{K_{IC}h^{1.5}b}\int_{\zeta_k}^{\xi} Y_P(\xi, \zeta_k)Y_M(\xi)\, d\xi - B\int_{\xi_r}^{\xi}\left[\int_{\max[\zeta_k,\zeta]}^{\xi} Y_P(y, \zeta_k)Y_P(y, \zeta)\, dy\right]\frac{\sigma[w(\zeta)]}{\sigma_u}\, d\zeta\right\} \quad (17)$$

In the case of discontinuous reinforcements, (7), (14), and (17) can be consistently applied provided the closing tractions are substituted by localized forces and the integrals by summations over the discrete number of the reinforcements.

The solution of the nonlinear integral problem is based on a discretization and an iterative procedure. By assuming a tentative crack face profile, the equilibrated cross-sectional configuration, for the crack at the onset of propagation, is calculated by the crack-propagation moment of (7) and the corresponding crack opening displacements of (17). If the equilibrated crack opening displacements are different from the assumed ones (according to a fixed tolerance) compatibility is not satisfied and the evaluated crack profile is assumed as the new tentative value. When the convergence is achieved, the crack-propagation moment of (7) and the localized rotation of (14) characterize the compatible and equilibrated solution (Carpinteri and Massabó, in press, 1996).

DIMENSIONLESS PARAMETERS

The analytical formulation proposed in the previous section has been developed in a dimensionless form to define, according to Buckingham's (1915) Theorem, the dimensionless parameters that synthetically control the behavior of the cross section in bending. A fundamental set of dimensionally independent variables, i.e. K_{IC} $[F][L]^{-1.5}$ and h $[L]$, has been chosen and the dimensionless products appearing in (7), (14), and (17), obtained by multiplying the different variables involved in the physical problem by a suitable combination of the fundamental set. In actual fact, the dimensionless crack-propagation moment $M_F/(K_{IC}h^{1.5}b)$ contains the cross-sectional thickness b, which can, however, be defined as a linear function of the cross-sectional depth h, if geometrical similarity is assumed.

The number of dimensionless parameters controlling the mechanical behavior depends at first on the assigned bridging or cohesive relation $\sigma(w)$. If this relation is rigid-plastic, $\sigma(w) = \sigma_u$, the closing tractions are uniform and constant along the fictitious crack faces, during the entire loading process. The traction-free crack depth ξ_r is equal to the depth of an initial notch. The constitutive flexural relationship can be evaluated through the equilibrium condition (7) alone. If the geometrical ratios are kept constant, the brittleness number B (i.e. N_P or s) proves to be the single parameter controlling the kind of behavior of the cross section.

On the other hand, for a generic bridging or cohesive law, with a critical crack opening displacement w_c, the problem is statically indeterminate and compatibility must be satisfied. To define the dimensionless parameters controlling the behavior for the above assumption, in addition to relations (7) and (17) reference must be made to the propagation condition for the traction-free crack, which controls the advancement of the bridging or cohesive zone. The traction-free crack propagates as soon as the crack opening displacement at its tip reaches the critical value w_c

$$\tilde{w}(\xi_r) = \tilde{w}_c \quad (18)$$

If $\tilde{E}$ is the dimensionless Young's modulus $\tilde{E} = (Eh^{0.5})/K_{IC}$, (17) and (18) yield

$$\frac{M_F}{K_{IC}h^{1.5}b}\int_{\xi_r}^{\xi} Y_P(\xi, \xi_r)Y_M(\xi)\, d\xi$$

$$- B\int_{\xi_r}^{\xi}\int_{\max[\xi_r,\zeta]}^{\xi} Y_P(y, \xi_r)Y_P(y, \zeta)\, dy\, \frac{\sigma[w(\zeta)]}{\sigma_u}\, d\zeta = \frac{1}{2}\tilde{E}\tilde{w}_c \quad (19)$$

This condition is verified at each iteration of the procedure described in the previous section. It points to the fact that, for an assigned generic bridging or cohesive law, if geometrical similarity is assumed, another dimensionless parameter, namely $\tilde{E}\tilde{w}_c = (Ew_c)/(K_{IC}h^{0.5})$, controls the composite flexural response. The functional constitutive relationship, linking the crack-propagation moment to the localized rotation, can be given the general form

$$f\left(\frac{M_F}{K_{IC}h^{1.5}b}, \phi, B, \tilde{E}\tilde{w}_c\right) = 0 \quad (20)$$

This relation has a general validity for both model options. Nevertheless, for the cohesive option, the brittleness number $B = 1/s$ and the parameter $\tilde{E}\tilde{w}_c$ are not independent variables. This is due to the relationship that exists between the homogenized fracture toughness of the composite, given by K_{IC} in the cohesive option and the fracture energy, $\mathcal{G}_F$

$$\mathcal{G}_F = \int_0^{w_c} \sigma(w)\, dw \quad (21)$$

$$K_{IC} = \sqrt{\mathcal{G}_F E} \quad (22)$$

On applying the power law (6*a*) to the preceding equations the relationship between the two dimensionless parameters becomes $\tilde{E}\tilde{w}_c = s(n + 1)/n$, while on applying the power law (6*b*) it becomes $\tilde{E}\tilde{w}_c = (n + 1)s$.

In conclusion, if the theoretical problem is analyzed via the bridging option of the proposed model, and the material is modeled as a multiphase, two dimensionless parameters, N_P and $\tilde{E}\tilde{w}_c$, control the mechanical response of the cross section. On the other hand, if the theoretical problem is analyzed via the cohesive option, which homogenizes the composite material, the sole dimensionless parameter s affects the kind of structural response. Physical similitude in the structural response is predicted when the mechanical and geometrical properties vary, as long as the dimensionless parameters are kept constant.

To verify these results, the cohesive option of the model has been applied assuming a linear relation, (6*a*) with $n = 1$, to analyze a beam with an initial notch of depth $a_0 = 0.1h$. In the dimensionless diagram $M_F/(K_{IC}h^{1.5}b)$ versus $(\phi Eh^{0.5})/K_{IC}$ of Fig. 2, different curves related to the brittleness numbers s = 5.0, 1.0, and 0.5, are shown. The shape of the curves changes from strain-hardening, for the greatest brittleness number s = 5.0, to strain-softening, for the lowest brittleness number s = 0.5. According to (9), an increase in the beam depth corresponds to a decrease in the brittleness number, if the mechanical properties are kept unchanged, and therefore the theoretical model predicts a size-scale effect characterized by a ductile-brittle transition. This kind of behavior, typical of quasi-brittle materials, such as concrete, mortar, or rocks, have been widely observed and theoretically reproduced (see, for instance, Carpinteri 1989).

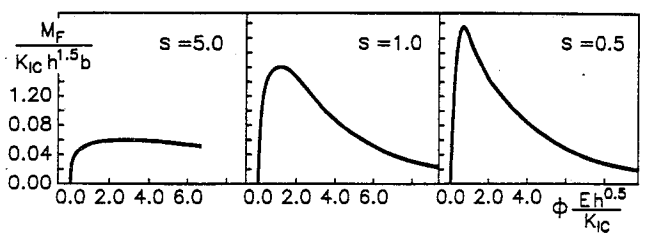

FIG. 2. Relationships between Dimensionless Moment and Normalized Rotation for Composite Characterized by Linear Decreasing Cohesive Relation; *s* from (9)

LIMIT BEHAVIOR: SMALL-SCALE BRIDGING CONDITION

The small-scale bridging condition for brittle-matrix composites assumes the existence of a process or bridging zone at the tip of the traction-free crack, which is small in relation to the crack size and the body dimensions.

Under particular conditions of the mechanical and geometrical properties of the composite cross section in bending (e.g. large depth, low fracture toughness, or high ultimate strength) the small-scale bridging condition is verified, the crack faces can be assumed as stress-free, and linear elastic fracture mechanics (LEFM) is applicable for the analysis of the flexural response. The composite material behaves like a homogeneous and brittle material and its fracture behavior is controlled by a single parameter, i.e. the homogenized composite fracture energy or the corresponding critical stress intensity factor, which are related through Young's modulus. The analytic relationships of the proposed theoretical model simplify in this limit situation.

Cohesive Option

According to the cohesive option, the crack starts propagating when the global crack tip stress intensity factor $(K_{IM} - K_{I\sigma})$ vanishes, (3). When the small-scale bridging condition holds, the limit value of the stress intensity factor $K_{I\sigma}$ due to the closing tractions, given by (5), represents the critical stress intensity factor of the homogenized material, which has been called K_{IC} in the analytic formulation of the previous section. K_{IC} is a constant related to the composite fracture energy via (22). The dimensionless crack-propagation moment of (7) takes on the form

$$\frac{M_F}{K_{IC}h^{1.5}b} = \frac{1}{Y_M(\xi)} \quad (23)$$

and the localized rotation at the onset of propagation is

$$\phi = \frac{2K_{IC}}{Eh^{0.5}}\frac{1}{Y_M(\xi)}\int_0^{\xi} Y_M^2(\xi)\, d\xi \quad (24)$$

The relations (23) and (24) are the LEFM relationships for a perfectly brittle homogeneous material. In the dimensionless diagram $M_F/(K_{IC}h^{1.5}b)$ versus $(\phi Eh^{0.5})/K_{IC}$ of Fig. 3, a comparison between the small-scale bridging flexural relationship,

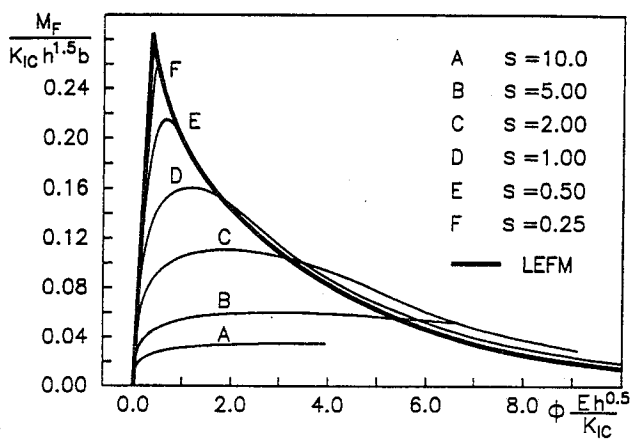

FIG. 3. Comparison between Small-Scale Bridging and Large-Scale Bridging Constitutive Flexural Relationships (Cohesive Option); *s* from (9)

thick curve, and the large-scale bridging relationships, thin curves, is shown. A cross section with an initial notch of depth $a_0 = 0.1h$ has been considered. The thin curves relate to different brittleness numbers, s = 10.00, 5.00, 2.00, 1.00, 0.50, and 0.25, and were obtained by the application of the cohesive option, assuming a linear decreasing law.

Fig. 3 brings out the well-known result according to which the ultimate loading capacity of the cross section and the entire curve predicted by a cohesive-crack model tend to the limit predicted by LEFM, when the brittleness number s decreases (i.e. h increases for unchanged mechanical properties). For decreasing values of s, the thin curves tend to draw nearer the LEFM curve after intersecting it. For brittleness numbers $s \leq 2$, the intersection points represent the beam configuration for which the traction-free crack starts propagating, and from that point on the LEFM macrostructural responses are almost coincident with the responses predicted by the cohesive option. On the other hand, the initial branches of the thin curves, as well as the peak values, differ from the ones predicted by LEFM, and are strongly dependent on both the brittleness number value and the shape of the assigned cohesive law. These branches reproduce the composite response during the loading phase in which the process zone is increasing and the shape of the crack faces is controlled by the cohesive tractions.

Fig. 3 brings out the fact that LEFM can be consistently applied for the description of the flexural response of members characterized by low brittleness numbers. On the other hand, LEFM can also be used with generic values of the brittleness number, for an approximate and conservative description of the constitutive branches beyond the intersection points. Application of the LEFM to predict the tail of the constitutive flexural relationship considerably simplifies the calculations connected with the nonlinear integral problem of the cohesive crack model, which involve iterative numerical processes that encounter great difficulty in reaching convergence and require considerable mesh refinements whether for low brittleness numbers or for high crack depth values.

Bridging Option

For the bridging option of the proposed theoretical model, arguments analogous to the preceding ones can be applied. In small-scale bridging condition, the energy required for the bridging mechanism to develop, during the formation of a unit increment of the crack surface area, $\mathcal{G}_b$ does not depend on the crack profile and is equal to the area under the bridging curve $\sigma_0(w)$. It is given by $\mathcal{G}_b = \alpha\rho\sigma_u w_c$, where α is a constant depending on the shape of the bridging law. If the power laws (6*a*,*b*) are assumed, α is equal to $n/(n + 1)$ or $1/(n + 1)$, respectively. Through (2), the dimensionless moment of crack propagation takes on the form

$$\frac{M_F}{K_{IC}h^{1.5}b} = \frac{1}{Y_M(\xi)}\sqrt{1 + \alpha\frac{\rho\sigma_u w_c E}{K_{IC}^2}} = \frac{1}{Y_M(\xi)}\sqrt{1 + \alpha N_P \tilde{E}\tilde{w}_c} \quad (25)$$

The localized rotation at the onset of crack propagation is

$$\phi = \frac{2K_{IC}}{Eh^{0.5}}\frac{1}{Y_M(\xi)}\sqrt{1 + \alpha N_P \tilde{E}\tilde{w}_c}\int_0^{\xi} Y_M^2(\xi)\, d\xi \quad (26)$$

Note that the term under the square root sign on the right-hand side of (25) and (26) is merely a function of the mechanical properties of the composite

$$\alpha N_P \tilde{E}\tilde{w}_c = \frac{G_b}{K_{IC}^2 E^{-1}} \quad (27)$$

Also in this case, as for the cohesive option, the constitutive flexural relationship given by (25) and (26) defines a limit curve in the dimensionless moment-versus-rotation diagram, which envelops the theoretical curves obtained in large-scale bridging by means of a bridged-crack model.

SIZE-SCALE EFFECT IN A BRITTLE-MATRIX COMPOSITE

In the flexural behavior of brittle-matrix composites, a size-scale effect is found, consisting of variations in the shape of the constitutive relationship when a characteristic dimension of the body varies. To analyze this phenomenon, the bridging option of the proposed theoretical model has been applied assuming a discontinuous bridging relation, $\sigma(w) = \rho\sigma_u$ if $w \leq w_c$, and $\sigma_0(w) = 0$ if $w > w_c$. This relation can represent the bridging mechanism of steel fibers with low yield stress and high aspect-ratio (see Burakiewicz 1978).

The flexural behavior of the cross section is controlled by the previously defined parameters N_P and $\tilde{E}\tilde{w}_c$. If only the size-scale effect is of interest, we can fix the bridging law and assume constant mechanical properties (K_{IC}, E, $\rho\sigma_u$, w_c). The product of the two dimensionless parameters, $N_P\tilde{E}\tilde{w}_c = (\rho\sigma_u E w_c)/K_{IC}^2$, which does not depend on the depth of the cross section, is then fixed.

The dimensionless moment-versus-localized rotation diagrams, $M_F/(K_{IC}h^{1.5}b)$ versus $(\phi E h^{0.5})/K_{IC}$, shown in Figs. 4, 5, and 6, relate to three different values of the parameter $N_P\tilde{E}\tilde{w}_c$, namely 36, 256, and 900. Beams with an initial matrix crack depth $a_0 = 0.1h$ crossed by unbroken fibers have been considered. The constitutive relationships have been calculated by following the evolution of the crack up to $a = 0.9h$. In each diagram a series of curves, for brittleness numbers N_P varying

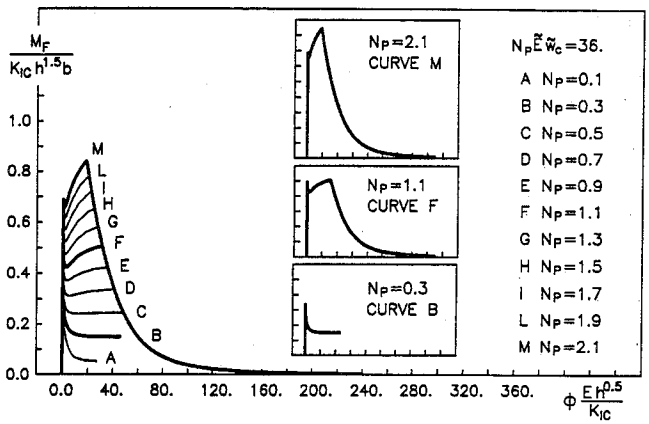

FIG. 4. Dimensionless Moment versus Rotation Diagram for Composite Characterized by Rectilinear Bridging Relation and $N_P\tilde{E}\tilde{w}_c = 36$

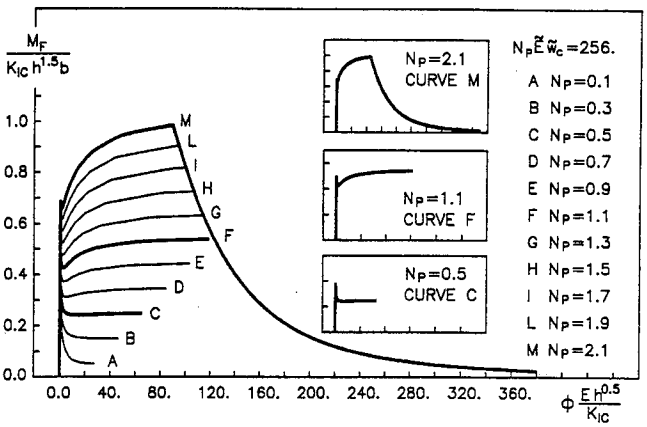

FIG. 5. Dimensionless Moment versus Rotation Diagram for Composite Characterized by Rectilinear Bridging Relation and $N_P\tilde{E}\tilde{w}_c = 256$

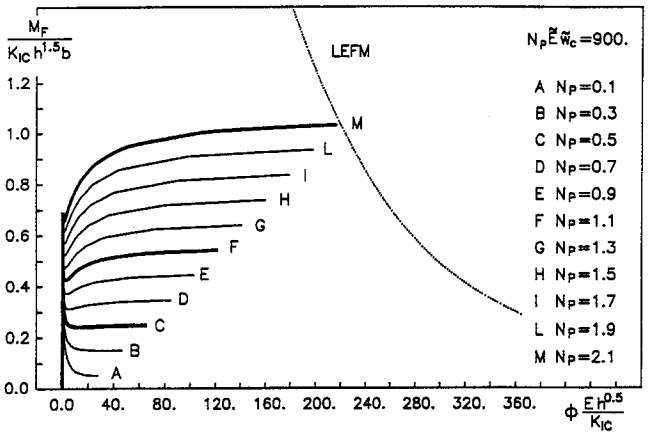

FIG. 6. Dimensionless Moment versus Rotation Diagram for Composite Characterized by Rectilinear Bridging Relation and $N_P\tilde{E}\tilde{w}_c = 900$

from 0.1 to 2.1, is depicted. Since the mechanical properties are kept unchanged, these curves represent the responses of beams of different depths. In particular, an increase in N_P means an increase in the beam depth, according to (8).

All of the curves in the diagrams of Figs. 4, 5, and 6 are characterized by three branches. The first is the linear-elastic branch describing the flexural response until the crack starts to propagate. The second branch depends on the brittleness number N_P and has been evaluated by applying the bridging option. It describes the beam behavior in large-scale bridging, namely when the bridging zone is invading the cross section and the crack is fully crossed by the fibers. The third unstable branch does not depend on the assumed brittleness number N_P, and has been evaluated using (25) and (26). It describes the behavior in small-scale bridging, when the traction-free crack propagates in the cross section. The small-scale bridging regime is controlled by the sole parameter $\alpha N_P\tilde{E}\tilde{w}_c$ of (27). As this parameter has been fixed for each figure, a single curve describes the third branch in all cases.

Let us first consider the diagrams shown in Fig. 5, which depict all of the probable behaviors. In the inset some curves are redrawn to highlight the variations in the structural response. The beam with $N_P = 0.5$ shows a hyperstrength phenomenon, i.e. a peak loading capacity greater than the ultimate loading capacity at total disconnection. The response of this beam in the first postcracking phase is strongly affected by the matrix fracture toughness, which prevails over the secondary phase toughening action controlling the ultimate loading capacity. The beam with $N_P = 1.1$ shows a snapthrough instability, which is an indication of an unstable crack advancement, arrested by the toughening action of the reinforcements. This instability would be represented by a jump at constant load if the process were controlled by the applied moment. After the discontinuity, the strain-hardening branch is controlled by the toughening action of the reinforcements that cross the crack up to total disconnection of the beam. The beam with $N_P = 2.1$ reaches the third unstable branch, which results in a catastrophic crack propagation, before complete disconnection.

The global responses of the beams with $N_P = 0.5$, $N_P = 1.1$, and $N_P = 2.1$ are strain-softening, strain-hardening, and strain-softening, respectively. This composite material is therefore characterized by a size-scale effect represented by a double transition in the flexural behavior, brittle to ductile, and then the reversal, ductile to brittle.

To estimate the kind of effects the double transition can have on the design of the structural components, consider a steel fiber-reinforced cementitious material with $K_{IC} = 50$ N/mm$^{1.5}$, $E = 40{,}000$ N/mm^2, $\rho = 0.02$, $\sigma_u = 200$ N/mm^2, and $w_c = 4$ mm. This results in a value of $N_P\tilde{E}\tilde{w}_c$ equal to 256. The curves in the inset characterize the constitutive flexural behavior of three beams made of this composite, and of different depths, $h \simeq 40$ mm, $h \simeq 190$ mm, and $h \simeq 690$ mm, respectively. The depths of the first two beams are in the range normally covered by the laboratory specimens and in this range a typical brittle-ductile transition is predicted when the beam depth increases. Experimental results of this kind have been obtained by Jamet et al. (1996) on fiber-reinforced concrete beams. However, in the steel fiber reinforced composite under consideration a new dangerous ductile-brittle transition is predicted when the beam depth increases. The largest beam considered, which could represent a real structural component, shows a strain-softening behavior (see Fig. 5).

When the mechanical properties of the beam are varied, the structural responses show substantial alterations. In the diagrams of Fig. 4, obtained for the lowest value of $N_P\tilde{E}\tilde{w}_c$, strain-softening behavior is predicted for all brittleness numbers. The low value of $N_P\tilde{E}\tilde{w}_c$ may be due to a small critical crack opening displacement, to a low fiber volume ratio, or to a high matrix fracture toughness.

On the other hand, in the diagrams of Fig. 6, obtained for a higher value of $N_P\tilde{E}\tilde{w}_c$, the structural responses vary from strain-softening to strain-hardening when the brittleness number increases, so that a brittle-ductile scaling transition is predicted. The LEFM curve, shown in the diagram of Fig. 6, does not intersect the different curves obtained in large-scale bridging; for this reason, the second ductile-brittle transition, shown by the previously examined material, does not appear in the range of the brittleness numbers considered. The thick curves in Fig. 6 represent, for example, the behavior of a fiber-reinforced cementitious material with $K_{IC} = 25$ N/mm$^{1.5}$, $E = 40{,}000$ N/mm^2, $\rho = 0.01$, $\sigma_u = 200$ N/mm^2, $w_c = 7$ mm and beam depths of $h \simeq 40$ mm, $h \simeq 190$ mm, and $h \simeq 690$ mm, respectively. The flexural responses in Fig. 6 coincide with the ones of a composite reinforced with fibers characterized by a rigid-perfectly plastic bridging relationship, for which the brittleness number N_P is the single governing parameter.

It is worth noticing that the reversal in the failure scaling transition is predicted even if a bridging law different from the rectilinear law is assumed. This is the case of (6*a*) with $n = 0.5$, which can be used to describe the pull-out of short steel fibers. The corresponding constitutive relationships are generally smoother and, as a consequence, the two elementary crises, for brittle crack growth and fiber yielding or pull-out, are not clearly differentiated in the overall responses. Note also that results similar to the ones previously shown can be obtained by the application of the cohesive option, provided the cohesive law is characterized by two parts, the former representing the matrix toughening action and the latter the fiber toughening action, such as a bilinear law (Carpinteri and Massabó, in press). For high-reinforced beams, the compressive crushing, neglected by the proposed model, could play an important role. Further studies are needed.

In conclusion, the proposed theoretical model predicts that for each brittle-matrix composite material of known mechanical properties and bridging mechanism, there exists a critical beam depth (or a critical N_P) beyond which the flexural responses change from being globally stable to globally unstable. The existence of this critical value in the range of depths embracing the laboratory samples and the actual structural components, depends on the properties of the composite material and on the position assumed by the LEFM curve in the dimensionless moment-versus-rotation diagram. It is therefore evident that the composition of the composite (kind of matrix and fibers and their volume ratio) can be suitably designed to avoid the dangerous ductile to brittle transition.

APPLICATIONS

The proposed theoretical model has been checked by simulating some experimental tests carried out on fiber-reinforced mortar beams by Jenq and Shah (1986). The beams, loaded in a three-point bending scheme, have a depth × thickness × span of 76 × 19 × 280 mm and a notch of depth $a_0 \simeq 25$ mm. The unreinforced matrix fracture toughness is equal to $K_{IC} = 27.5$ N/mm$^{1.5}$, and Young's modulus has been evaluated to be 22,000 N/mm^2. Brass-coated smooth steel fibers, 25 mm long and with a 0.4 mm diameter, were used in three different volume ratios $\rho = 0.005$, 0.010, and 0.015. The pull-out response of the single aligned fiber shows the typical frictional behavior. The power law $\sigma(w) = \sigma_u(1 - w/w_c)^2$ has been proposed by Jenq and Shah to model the experimental results, where $\sigma_u = 169$ N/mm^2 is the maximum pull-out strength and w_c is the critical crack opening displacement, equal to half the fiber length.

To apply the bridging option of the theoretical model, the dimensionless parameters N_P and $\tilde{E}\tilde{w}_c$, and the bridging relation $\sigma_0(w)$ have to be defined. Eqs. (20) and (8) give $\tilde{E}\tilde{w}_c = 1{,}147$ and $N_P = 0.27$, 0.54, and 0.80, for $\rho = 0.005$, 0.010, and 0.015, respectively. As a first approximation, the bridging law $\sigma_0(w)$ for all the fibers has been defined as the product of the fiber volume ratio ρ and $\sigma(w)$, given by the previously mentioned power law. To evaluate the load-deflection theoretical curves, the constitutive moment-versus-localized rotation relationship of (14) has been used to characterize a nonlinear hinge placed in the middle free span of a three-point bending linear-elastic beam.

Fig. 7 shows the relationship between the applied load P and the middle-span deflection δ. The thin curves represent the experimental results, while the thick curves the theoretical ones. Fig. 7(a) refers to the underreinforced beam ($\rho = 0.005$). It is observed that the global strain-softening behavior and the hyper-strength phenomenon of the beam are faithfully reproduced by the model, and are accounted for by the low brittleness number $N_P = 0.27$.

Fig. 7(b,c) refer to the beams with $\rho = 0.010$ and 0.015, characterized by an elasto-plastic and a strain-hardening response, respectively. The theoretical curves, with $N_P = 0.54$ and 0.80, are represented by the dashed lines in the diagrams. These curves do not reproduce the postcracking responses satisfactorily and the predicted ultimate loads are lower than the experimentally determined values. These discrepancies cannot be due to an erroneous modeling of the mortar fracture toughness, as it does not control the ultimate loading capacity. Moreover, they cannot be due to an erroneous modeling of the shape of the bridging law $\sigma(w)$, because it does not affect the response when the crack mouth opening displacement (CMOD) remains very small, as is the case in the previously mentioned beams (see Fig. 8). Therefore, the differences between the experimental and the theoretical curves can be only due to an erroneous assumption of the maximum value, $\rho\sigma_u$, of the bridging law $\sigma_0(w)$.

The maximum pull-out value was obtained assuming that all of the fibers were pulled out along their alignment. In actual fiber-reinforced beams the fibers are usually pulled out off-axes during crack propagation. In high-fiber volume ratio beams, the preceding fact usually leads to an increase in the maximum pull-out load (Ouyang et al. 1994). The higher pull-out load can be accounted for by assuming a higher effective fiber volume ratio ρ_e. The discrepancies between the theoretical and the experimental values in Fig. 7(b,c) disappear on assuming $\rho_e = 0.014$ and $\rho_e = 0.020$, respectively. The corresponding brittleness numbers become $N_P = 0.75$ and 1.08.

Fig. 8(a) shows the dimensionless moment-versus-rotation diagram of an unreinforced mortar beam. The theoretical curve has been obtained by means of the LEFM (23) and (24). Apart from the prepeak loading phase, controlled by microcracking phenomena neglected by LEFM, and the peak value, which is greater than the real one, a good agreement is found between the two curves.

In Fig. 8(b), the experimental and theoretical curves, relating the applied load to CMOD, are shown for the three beams. The good fit obtained confirms the preceding results. Also note that, for all the tested beams, the bridging zone extends over the entire length of the crack even at total disconnection

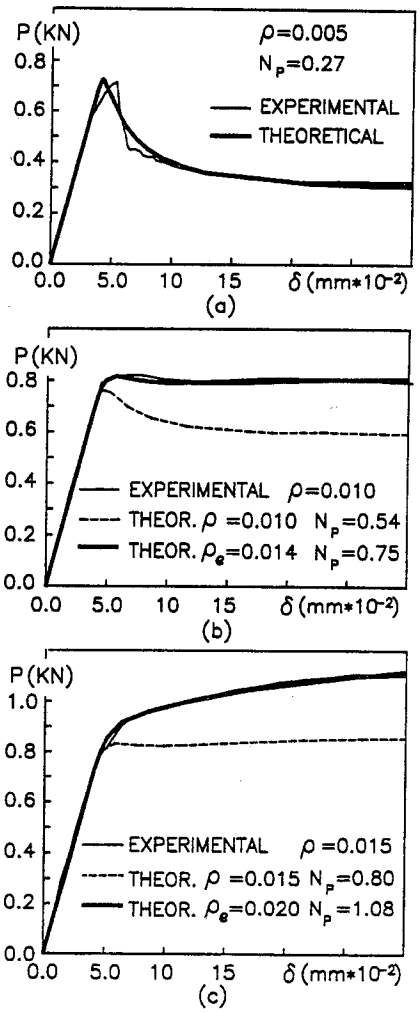

FIG. 7. Load versus Deflection Curves for Fiber-Reinforced Mortar Beams [Comparison between Experimental (Jenq and Shah 1986) and Theoretical Results (Bridging Option)]

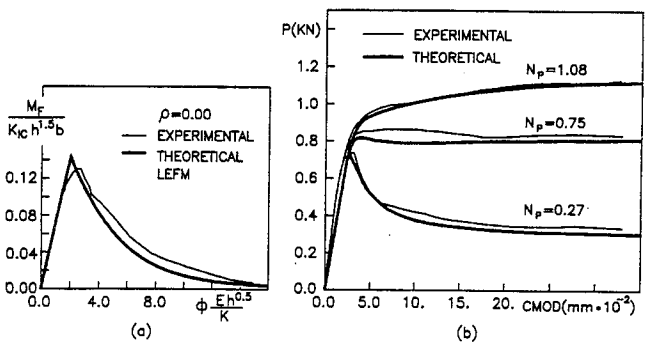

FIG. 8. Comparison between Experimental (Jenq and Shah 1986) and Theoretical Results of: (a) Dimensionless Moment versus Rotation Curves for Mortar Beam in Bending (LEFM); (b) Load versus Crack Mouth Opening Displacement Curves for Fiber-Reinforced Mortar Beams (Bridging Option)

(CMOD < w_c). This fact explains the observed globally stable structural responses (see Fig. 6).

It is worth noticing that the application of the cohesive option of the proposed model would have led to the same theoretical results, provided the cohesive law $\sigma_0(w)$, describing the homogenized composite toughening mechanism, were properly defined. This result has been proved by Carpinteri and Massabó (in press, 1996), by assuming a bilinear cohesive law with a sharp drop and a long tail.

CONCLUSIONS

A nondimensional fracture mechanics model has been proposed for analysis of the flexural behavior of brittle-matrix composites with uniformly distributed secondary phases. It has been shown that the flexural behavior of geometrically similar structures is controlled by one dimensionless parameter, if the composite is modeled as a monophase material, or by two dimensionless parameters, when modeled as a multiphase material.

In the first case the toughening mechanism of the homogenized composite is represented by a closing traction distribution (cohesive tractions), acting along a fictitious crack, and linked to the crack opening displacement by a cohesive relation. In the second case the toughening mechanisms related to the different phases are separately modeled: a critical stress intensity factor reproduces the matrix fracture toughness, and a distribution of closing tractions (bridging tractions), reproduces the secondary-phase restraining action.

On modeling the composite as a monophase, with cohesive tractions that are linearly decreasing functions of the crack opening displacement, a ductile-brittle transition in the flexural response of the beam is predicted, when the depth increases. This behavior is typical of quasi-brittle materials.

On the other hand, on modeling the composite as a multiphase with bridging tractions characterized by a rigid-plastic relation, a brittle-ductile transition is predicted in the flexural behavior. Nevertheless, if the bridging law in the above case has a critical crack opening displacement, beyond which the tractions vanish, the composite undergoes a double brittle-ductile-brittle transition. This behavior can take place in the flexural response of fiber-reinforced cementitious materials. The appearance of the transition reversal over the dimensional range embracing the laboratory specimens and the actual structural components, depends on the composite mechanical properties and on the kind of law governing the toughening mechanisms.

ACKNOWLEDGMENTS

The authors gratefully acknowledge the financial support of the National Research Council (CNR) and the Department for the University and for Scientific and Technological Research (MURST).

APPENDIX. REFERENCES

Ballarini, R., Shah, S. P., and Keer, L. M. (1984). "Crack growth in cement-based composites." *Engrg. Fracture Mech.*, 20(3), 433–445.

Barenblatt, G. I. (1959). "The formation of equilibrium cracks during brittle fracture. General ideas and hypotheses. Axially-symmetric cracks." *J. Appl. Math. Mech.*, 23(3), 622–636.

Barenblatt, G. I. (1962). "The mathematical theory of equilibrium cracks in brittle fracture." *Advances in applied mechanics*, H. L. Dryden and T. von Karman, eds., Academic Press, Inc., New York, N.Y., 55–129.

Bosco, C., Carpinteri, A., and Debernardi, P. G. (1990). "Minimum reinforcement in high-strength concrete." *J. Struct. Engrg.*, ASCE, 116(2), 427–437.

Bosco, C., and Carpinteri, A. (1992). "Softening and snap-through behavior of reinforced elements." *J. Engrg. Mech.*, ASCE, 118(8), 1564–1577.

Bosco, C., and Carpinteri, A. (1995). "Discontinuous constitutive response of brittle matrix fibrous composites." *J. Mech. Phys. Solids*, 43(2), 261–274.

Buckingham, E. (1915). "Model experiments and the form of empirical equations." *Trans. ASME*, 37(1487), 263–296.

Burakiewicz, A. (1978). "Testing of fibre bond strength in cement matrix." *Testing and test methods of fiber cement composites*, R. N. Swamy, ed., The Construction Press, Ltd., Lancaster, U.K., 355–369.

Carpinteri, A. (1981). "Static and energetic fracture parameters for rocks and concretes." *Mat. and Struct.*, 14(81), 151–162.

Carpinteri, A. (1984). "Stability of fracturing process in r.c. beams." *J. Struct. Engrg.*, 110(3), 544–558.

Carpinteri, A. (1989). "Cusp catastrophe interpretation of fracture instability." *J. Mech. Phys. Solids*, 37(5), 567–582.

Carpinteri, A., and Massabó, R. (1995). "Nonlinear fracture mechanics models for fibre reinforced materials." *Proc., Int. Symp. on Advanced Technol. for Des. and Fabrication of Composite Mat. and Struct.*, G. C. Sih, A. Carpinteri, and G. Surace, eds., Kluwer Academic Publishers, Dordrecht, The Netherlands, 31–48.

Cotterell, B., Paramasivam, P., and Lam, K. Y. (1992). "Modelling the fracture of cementitious materials." *Mat. and Struct.*, 25(145), 14–20.

Cox, B. N., and Marshall, D. B. (1994). "Concepts for bridged cracks in fracture and fatigue." *Acta Metallurgica Materialia*, 42(2), 341–363.

Desayi, P., and Ganesan, N. (1986). "Fracture behavior of ferrocement beams." *J. Struct. Engrg.*, 112(7), 1509–1525.

Dugdale, D. S. (1960). "Yielding of steel sheets containing slits." *J. Mech. Phys. Solids*, 8(2), 100–104.

Foote, R. M. L., Mai, Y.-W., and Cotterell, B. (1986). "Crack growth resistance curves in strain-softening materials." *J. Mech. Phys. Solids*, 34(6), 593–607.

Hillerborg, A., Mooder, M., and Petersson, P. E. (1976). "Analysis of crack formation and crack growth in concrete by means of fracture mechanics and finite elements." *Cement and Concrete Res.*, 6(6), 773–782.

Hillerborg, A. (1989). "Analysis of fracture by means of the fictitious crack model, particularly for fibre reinforced concrete." *Int. J. Cement Composites*, 2(4) 177–184.

Jamet, D., Gettu, R., Gopalaratnam, V. S., and Aguado, A. (1996). "Toughness of fiber-reinforced high-strength concrete from notched beam tests." in *Testing of fiber reinforced concrete*, eds., D. J. Stevens et al., SP-155, ACI Detroit, 23–29.

Jenq, Y. S., and Shah, S. P. (1985). "Two parameter fracture model for concrete." *J. Engrg. Mech.*, 111(10), 1227–1241.

Jenq, Y. S., and Shah, S. P. (1986). "Crack propagation in fiber-reinforced concrete." *J. Struct. Engrg.*, 112(1), 19–34.

Li, V. C., and Liang, E. (1986). "Fracture processes in concrete and fiber reinforced cementitious composites." *J. Engrg. Mech.*, 112(6), 566–586.

Mai, Y. W. (1985). "Fracture measurements for cementitious composites." *Application of fracture mechanics to cementitious composites*, S. P. Shah, ed., Martinus Nijhoff Publishers, Dordrecht, The Netherlands, 399–429.

Ouyang, C., Pacios, A., and Shah, S. P. (1994). "Pullout of inclined fibers from cementitious matrix." *J. Engrg. Mech.*, 120(12), 2641–2659.

Romualdi, J. P., and Batson, G. B. (1963). "Behavior of reinforced concrete beams with closely spaced reinforcements." *ACI J.*, 60(6), 775–789.

Shah, S. P. (1988). "Fracture toughness of cement-based materials." *Mat. and Struct.*, 21(122), 145–150.

Tada, H., Paris, P. C., and Irwin, G. (1985). *The stress analysis of cracks handbook*. Paris Productions Incorporated (and Del Research Corporation), St. Louis, Mo.

Visalvanich, K., and Naaman, A. E. (1983). "Fracture model for fiber reinforced concrete." *ACI J.*, 80(2), 128–138.

Wecharatana, M., and Shah, S. P. (1983). "A model predicting fracture resistance of fiber reinforced concrete." *Cement and Concrete Res.*, 13(6), 819–829.